Amino terminal glutamate residues confer spermine sensitivity and affect voltage gating and channel conductance of rat connexin40 gap junctions

Hassan Musa[1], Edward Fenn[1], Mark Crye[1], Joanna Gemel[2], Eric C. Beyer[2] and Richard D. Veenstra[1]

[1]*Department of Pharmacology, SUNY Upstate Medical University, Syracuse, NY 13210, USA*
[2]*Department of Pediatrics, University of Chicago, Chicago, IL 60637, USA*

Connexin40 (Cx40) contains a specific binding site for spermine (affinity ∼100 μM) whereas connexin43 (Cx43) is unaffected by identical concentrations of intracellular spermine. Replacement of two unique glutamate residues, E9 and E13, from the cytoplasmic amino terminal domain of Cx40 with the corresponding lysine residues from Cx43 eliminated the block by 2 mM spermine, reduced the transjunctional voltage (V_j) gating sensitivity, and reduced the unitary conductance of this Cx40E9,13K gap junction channel protein. The single point mutations, Cx40E9K and Cx40E13K, predominantly affected the residual conductance state (G_{min}) and V_j gating properties, respectively. Heterotypic pairing of Cx40E9,13K with wild-type Cx40 in murine neuro2A (N2A) cells produced a strongly rectifying gap junction reminiscent of the inward rectification properties of the Kir (e.g. Kir2.x) family of potassium channels. The reciprocal Cx43K9,13E mutant protein exhibited reduced V_j sensitivity, but displayed much less rectification in heterotypic pairings with wtCx43, negligible changes in the unitary channel conductance, and remained insensitive to spermine block. These data indicate that the connexin40 amino terminus may form a critical cytoplasmic pore-forming domain that serves as the receptor for V_j-dependent closure and block by intracellular polyamines. Functional reciprocity between Cx40 and Cx43 gap junctions involves other amino acid residues in addition to the E or K 9 and 13 loci located on the amino terminal domain of these two connexins.

(Received 9 December 2003; accepted after revision 23 April 2004; first published online 23 April 2004)
Corresponding author R. D. Veenstra: Department of Pharmacology, SUNY Upstate Medical University, Syracuse, NY 13210, USA. Email: veenstrr@upstate.edu

Gap junctions mediate homeostatic electrical and chemical coupling by forming aqueous pores between like cell types that are typically open under resting conditions. Gap junction conductance (g_j) is modulated by a variety of cellular signals including transjunctional differences in membrane potential (V_j), intracellular calcium, intracellular pH, serine/threonine and tyrosine kinases (e.g. mitosis-associated protein kinase (MAPK) and c-src), and, most recently, intracellular polyamine (i.e. spermine) levels (Harris, 2001; Lampe & Lau, 2000; Musa & Veenstra, 2003). The polyamines are endogenous to all eukaryotic cells and are required for cell proliferation due to their DNA binding properties (Tabor & Tabor, 1984). These same polyamines regulate cellular membrane potential by blocking the inward rectifier potassium channels (Kir2.x) at depolarized potentials whereas delayed rectifier potassium channels (Kv1–4.x) are activated by membrane voltage (V_m). The polyamines, of which spermine is the most potent, also modulate chemical synaptic transmission by modulating the activity of several ligand-gated ion channel receptors including the *N*-methyl-D-asparate (NMDA), AMPA/kainate glutamate (GluR), and nicotinic acetylcholine (nAChR) receptor channels (Williams, 1997). Intracellular calcium signalling is similarly inhibited since spermine blocks the rod cyclic nucleotide gated (CNG) and ryanodine (RyR) receptor channels (Uehara *et al.* 1996; Lu & Ding, 1999). The most common mechanism of action is blockade of the ion permeation pathway by interactions with acidic or neutral glutamate, glutamine, aspartate, or asparagine amino acids within the channel pore (Ficker *et al.* 1994; Lopatin *et al.* 1994; Bowie & Mayer, 1995; Chao *et al.* 1997; Guo & Lu, 2000*a*). These sites are critical to the ionic selectivity filter and their blockade is characterized by reductions in

 DOI: 10.1113/jphysiol.2003.059386

open channel conductance often manifested as flickery channel block (Hume *et al.* 1991; Mori *et al.* 1992; Root & MacKinnon, 1993; Wible *et al.* 1994; Abrams *et al.* 1996). Blockade or stimulation at more external sites involved in channel gating, best characterized by reductions or increases in channel open probability, have also been observed in multiple channel types (Yang *et al.* 1995; Hurst *et al.* 1995; Kashiwagi *et al.* 1996). Spermine is the only polyamine known to significantly reduce g_j in the physiological submillimolar range in connexin40 (Cx40), but not connexin43 (Cx43), gap junctions (Musa & Veenstra, 2003). In this study, we examined the functional consequences of the natural occurrence of glutamate or lysine residues at positions 9 and 13 of Cx40 and Cx43, respectively. We describe the existence of a very specific 'glutamate-or-lysine switch' between Cx40 and Cx43 that eliminates the spermine blocking properties of Cx40 gap junctions. This glutamate-or-lysine (E/K) switch resides on the cytoplasmic amino terminal (NT) domain of the connexins. In addition to the elimination of the block by spermine, the K-for-E substitutions in Cx40 had pronounced effects on the V_j gating and unitary channel conductance properties of Cx40 gap junctions.

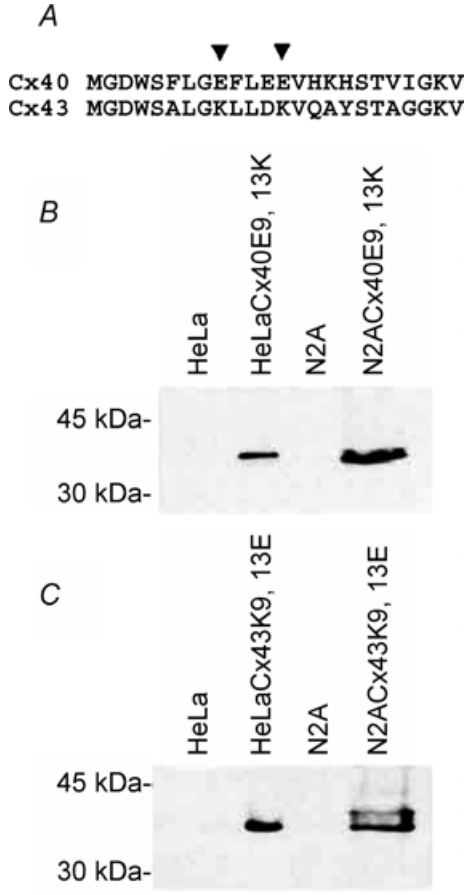

Figure 1. Differing amino acids in the amino terminal domain of Cx40 and Cx43 and expression of site-directed mutants
A, primary amino acid sequences of the first 24 amino acids of Cx40 and Cx43. Arrowheads indicate the position of the two reciprocal point mutations introduced into Cx40 (Cx40E9,13K) and Cx43 (Cx43K9,13E). *B* and *C*, immunoblot detection of Cx40E9,13K and Cx43K9,13E protein production 72 h after transient transfection with the pcDNA3. 1-neo vector construct. Protein extracts from HeLa (10 μg) or N2A (100 μg) cells were separated by SDS-PAGE, transferred to nylon membranes, and detected using connexin specific rabbit polyclonal antibodies.

Methods

N2A cell transfection with mutant connexin40 and connexin43 cDNA constructs

Stable wild-type (wt) Cx40- and Cx43-transfected mouse neuro2A (N2A) cell cultures were prepared and maintained as previously described (Beblo *et al.* 1995). The mutant DNAs were generated using PCR site-directed mutagenesis according to established protocols (Vallette *et al.* 1989). The primary amino acid sequences for the cytoplasmic amino terminal (NT) domain of Cx40 and Cx43 are shown in Fig. 1*A*. The two glutamate (E) or lysine (K) residues present in Cx40 or Cx43, respectively, at positions 9 and 13, indicated by the arrowheads, were reciprocally mutated to generate the Cx40E9,13K and Cx43K9,13E double point mutations and the Cx40E9K, Cx40E13K, Cx43K9E, and Cx43K13E single point mutations. The mutant cDNAs were cloned into the pTracer^{TM}-CMV2 vector (Invitrogen) using the Kpn1 and Xba1 sites. The plasmid construct was purified using a Plasmid Maxi Kit (Qiagen) and the sequence confirmed. Transient transfections were performed on N2A cells grown to 80–90% confluency in a 24-well culture dish (Falcon) using Lipofectamine^{TM} 2000 (Invitrogen) according to the manufacturer's instructions.

Western blot analysis

Expression of mutant connexin proteins was confirmed by immunoblotting using Cx40- and Cx43-specific antibodies (Fig. 1*B* and *C*). N2A cells were harvested 72 h after transfection. Protein extracts from cells were prepared as described by Laing & Beyer (1995). Aliquots containing 10 μg of protein from parental or transfected HeLa and 100 μg of protein from parental or transfected N2A cells were separated by SDS-PAGE on 10% polyacrylamide gels and blotted onto Immobilon-P membranes (Millipore).

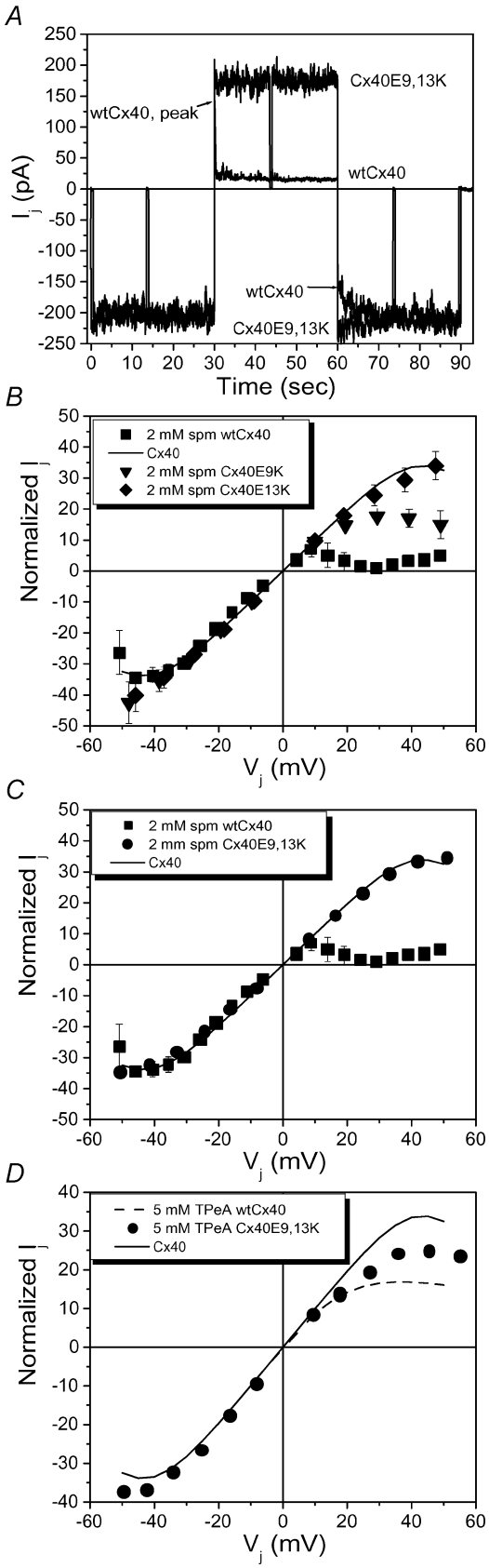

Connexin-specific protein was detected using a rabbit antiserum directed against a bacterially expressed Cx40 carboxyl tail fusion protein (1 : 5000 dilution) or GST-Cx43 C-terminal fusion protein (1 : 20 000) (Kwong *et al.* 1998). Peroxidase conjugated goat anti-rabbit IgG (1 : 5000 dilution) was used as a secondary antibody. Immunoblots were developed with electrogenerated chemiluminiscence (ECL) reagents following the manufacturer's instructions (Amersham).

Electrophysiological recording

N2A cell cultures were washed 3–5 times with Hepes-buffered saline and placed on the stage of an inverted phase contrast microscope (Olympus IMT-2, Lake Success, NY, USA). The bath saline contained (mM): 142 NaCl, 1.3 KCl, 0.8 $MgSO_4$, 0.9 NaH_2PO_4, 1.8 $CaCl_2$, 4.0 CsCl, 2.0 TEACl, 5.5 dextrose, 10 Hepes (pH 7.4, titrated with 1 N NaOH), 310 mosmol kg^{-1}. Junctional current recordings were obtained using conventional double whole-cell recording techniques with two Axopatch 1D (Axon Instruments, Union City, CA, USA) patch clamp amplifiers (Veenstra, 2001). Patch electrodes (PG52151-4, WPI, Inc., Sarasota, FL, USA) had tip resistances of 4–6 MΩ prior to gigaohm seal formation and patch break when filled with 140 mM KCl internal pipette solution (IPS). The standard KCl IPS contained (mM): 140 KCl, 4.0 CsCl, 2.0 TEACl, 3.0 $CaCl_2$, 5.0 K_4BAPTA, 1.0 $MgCl_2$, 25 Hepes (pH 7.4, titrated with 1 N KOH), 310 mosmol kg^{-1}. MgATP was added daily to

Figure 2. Effect of unilateral application of 2 mM spermine on wtCx40 and mutant Cx40 gap junctions
A, superimposed I_j traces from wtCx40 and Cx40E9,13K cell pairs showing responses to the −40/+40/−40 mV V_j steps with 2 mM spermine added to the patch pipette of the pulsed cell. I_j remained ohmic for the 30 s duration of each V_j step in Cx40E9,13K gap junctions compared to the significant reduction in wtCx40 I_j at +40 mV. A 0.5 s pulse to baseline ($V_j = 0$) was included in the middle of each V_j step. *B*, *I–V* relationships for the single point mutant Cx40E9K, Cx40E13K, and wtCx40 gap junctions in the presence of unilateral 2 mM spermine. The continuous line indicates the normal V_j-dependent gating of wtCx40 ($V_{½} = \pm 50$ mV, $z = 3.8$, and $G_{min} = 0.26$; Veenstra, 2001). This concentration of spermine blocks all positive I_j values in wtCx40, but with nominal or reduced effects on Cx40E13K and Cx40E9K gap junctions. *C*, unilateral 2 mM spermine *I–V* relationships for the double point mutant Cx40E9,13K gap junctions relative to wtCx40. *D*, *I–V* relationships for wtCx40 (model, dashed line; Musa *et al.* 2001) and Cx40E9,13K in the presence of 5 mM TPeA. In contrast to spermine, a significant degree of TPeA block is conserved in the Cx40E9,13K mutant.

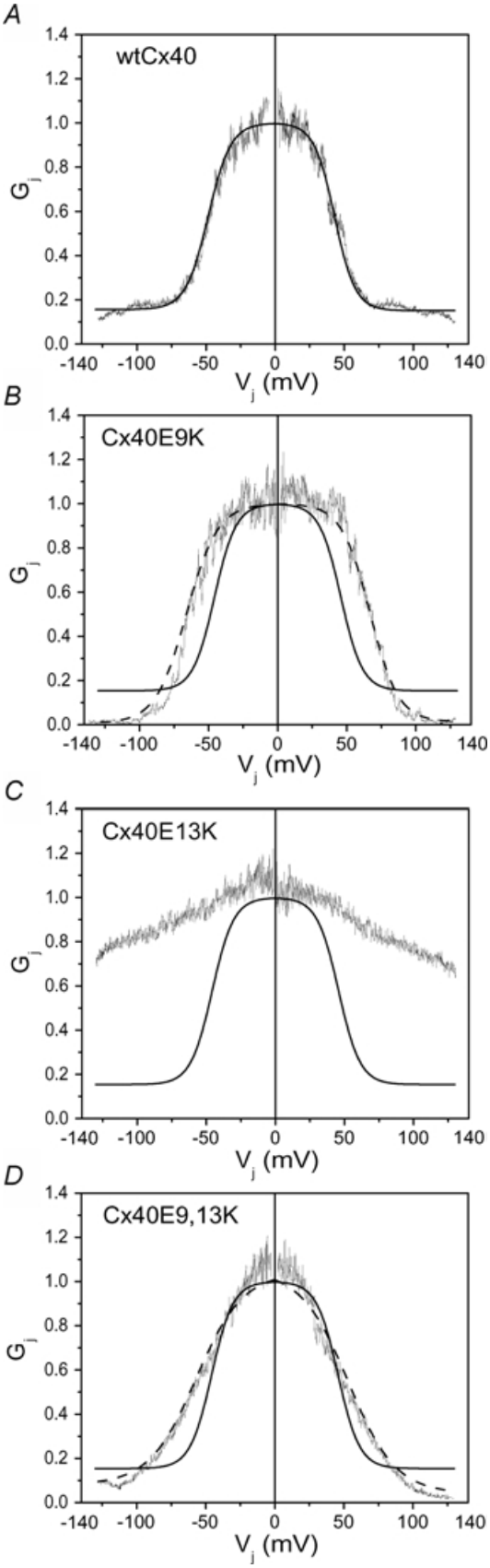

achieve a final concentration of 3.0 mM. All experiments were performed at room temperature (20–22°C). All currents were digitized at 1–4 kHz after low pass filtering at 100–500 Hz (LPF 202 A, Warner Institute, Hamden, CT, USA). Analysis and curve fitting procedures were performed using Clampfit software (pCLAMP version 8.2, Axon Instruments, Inc.) All curve fitting was performed using the sum of squared errors minimization procedure and the standard error for each estimated parameter are provided. Final graphs were prepared using Origin version 6.1 or 7.0 software (OriginLab Corporation, Northampton, MA, USA).

Normalized steady-state junctional *I–V* and *G–V* relationships were obtained with continuous 200 ms mV^{-1} voltage ramps where V_1 was varied from –40 to –140 or +60 mV in 1 mV increments (Veenstra, 2001). A rest interval of 15 s was included between each voltage ramp. Each V_1 ramp was repeated four to five times per experiment and the I_1 and I_2 traces were ensemble averaged prior to calculation of I_j and g_j. To ensure accuracy, quantitative methods were used to correct for junctional voltage errors resulting from the series resistance R_{el} of each patch electrode in the junctional conductance (g_j) calculations according to the expression:

$$g_j = \frac{-\Delta I_2}{V_1 - (I_1 R_{el1}) - V_2 + (I_2 R_{el2})} \quad (1)$$

A steady-state I_j–V_j relationship was obtained for each experiment and the maximum junctional conductance ($g_{j,max}$) was calculated from the slope of the linear regression fit of the –5 to –25 mV I_j–V_j curve for each experiment (Musa *et al.* 2001; Musa & Veenstra, 2003). The normalized junctional conductance ($G_j = g_j/g_{j,max}$) and I_j–V_j relationships ($= I_j/[g_{j,max} \times V_j]$) were determined

Figure 3. Transjunctional conductance–voltage curves for wt and mutant Cx40 gap junctions
A, the normalized steady-state junctional conductance–voltage (G_j–V_j) curve for wtCx40 gap junctions. The parameter values for the fitted Boltzmann distribution (continuous line) are provided in Table 1. *B*, the fitted G_j–V_j curve for Cx40E9K (dashed line) compared with wtCx40 (continuous line) gap junctions. The half-inactivation voltage ($V_{1/2}$) of Cx40E9K normalized G_j–V_j curve was shifted outward by 20 mV, the gating charge valence (z) reduced by 27%, and minimum G_j (G_{min}) reduced to zero compared to wtCx40 (continuous line) gap junctions. *C*, the fitted G_j–V_j curve for Cx40E13K (dashed line) compared to wtCx40 (continuous line) gap junctions. The Cx40E13K G_j–V_j relationship could not be fitted with a Boltzmann curve. *D*, the fitted G_j–V_j curve for Cx40E9,13K (dashed line) compared to wtCx40 (continuous line) gap junctions. The $V_{1/2}$ was increased by 10 mV, the gating charge valence (z) reduced by 54%, and the G_{min} reduced to 0.06 by the double Cx40E9,13K mutation.

Table 1. Boltzmann equation values for the Cx40 G_j–V_j curves

	wtCx40		Cx40E9K		Cx40E9,13K	
Parameter[a]	$-V_j$	$+V_j$	$-V_j$	$+V_j$	$-V_j$	$+V_j$
G_{max}	1.0[b]	1.0[b]	1.0[b]	1.0[b]	1.0[b]	1.0[b]
$V_{½}$ (mV)	-45.8 ± 3.8	$+45.8 \pm 3.8$	-65.9 ± 0.1	$+66.8 \pm 0.1$	-57.1 ± 0.2	$+53.2 \pm 0.2$
z	-3.88 ± 0.25	3.88 ± 0.25	-2.70 ± 0.03	2.95 ± 0.03	-1.79 ± 0.02	1.77 ± 0.02
G_{min}	0.15 ± 0.004	0.15 ± 0.004	0.008 ± 0.002	0.013 ± 0.002	0.08 ± 0.003	0.04 ± 0.003

[a]The steady-state junctional G–V curves were fitted with eqn (2) to obtain the above parameters:

$$G_j = G_{min} + \frac{G_{max} - G_{min}}{1 + \exp[(zF/RT)(V_j - V_{1/2})]}$$

[b]G_{max} was fixed to a value of 1.0 since all junctional conductance measurements were normalized to the maximum g_j for each experiment. Values are means ± S.E.M.

according to each experimental $g_{j,max}$ value. The data from three to five experiments were pooled for each experimental group.

Ionic blockade experiments

Spermine and tetrapentylammonium (TPeA) salts were added unilaterally as indicated for each experiment. Spermine HCl (Calbiochem, La Jolla, CA, USA) and TPeACl (Aldrich Chem Co., Milwaukee, WI, USA) were stored at –20°C as 500 mM stock solutions in 18 MΩ cm water and diluted daily as required with KCl IPS. The final osmolarity of the TPeA + KCl IPS was not adjusted since the maximum dose of 5 mM TPeA altered the final IPS volume by 1% and the total osmolarity by 3% (Musa *et al.* 2001). For most spermine concentrations, the IPS osmolarity was altered by ∼1% (Musa & Veenstra, 2003). To determine the magnitude of polyamine (PA) block, a voltage protocol that sequentially altered the holding potential (ΔV_1) of the PACl + KCl-containing cell (cell 1) from negative to positive and back to negative potentials relative to the KCl-containing cell (cell 2) in 30 s intervals was used. The common holding potential (V_1 and V_2) was –40 mV for both cells. Cell 1 was stepped to this common potential for 0.5 s during each V_j step and for 10 s between different –/+/–command voltages to assess any change in the non-junctional voltage clamp circuit. $V_j = (V_1 + \Delta V_1) - V_2$ and ΔV_1 was altered in 5 or 10 mV increments from 5 to 50 mV and $I_j = -\Delta I_2$.

Results

Effects of connexin40 E-to-K mutations on ionic blockade

Double whole-cell patch clamp recordings of gap junction currents (I_j) were obtained from homotypic pairs of connexin-transfected N2A cells after 24 h. The V_m of one cell (cell 1) was varied and the difference in whole-cell current of the second cell (cell 2) represented the negative of the net I_j ($\Delta I_2 = -I_j$, Veenstra, 2001). The unilateral addition of 2 mM spermine to the patch pipette of cell 1 achieved maximum block in wild-type (wt) Cx40 cell pairs (Fig. 2*A*–*C*). The same protocol failed to block I_j in Cx40E9,13K and Cx40E13K cell pairs, with intermediate amounts of block evident at $V_j \leq +50$ mV in Cx40E9K cell pairs (Fig. 2*B* and *C*). Further reductions in Cx40E9K I_j with 2 mM spermine at higher V_j values were complicated by the V_j gating present in these homotypic gap junctions above ±50 mV (see Fig. 3*B* and Table 1). We were unable to determine the voltage-dependent dissociation constants ($K_m(V_j)$) for spermine blockade of this Cx40E9K gap junction since significantly less block was observed in the presence of unilateral 0.5 and 1.0 mM spermine. The decreased blockade near 0 mV in the mutant Cx40 gap junctions indicates that the tetravalent spermine molecule associates predominantly with the E13 locus, and to a lesser extent with the E9 locus, on the NT domain of Cx40.

Tetrapentylammonium (TPeA) ions are known to reduce both Cx40 and Cx43 I_j in a V_j-dependent manner (Veenstra, 2000; Musa *et al.* 2001). Although TPeA only produces partial blockade and acts as a permeable blocker of wtCx40 I_j, presumably by hindering ionic currents owing to its large diameter (>10 Å, 1 nm), it provides another independent test of the cation permeation pathway of gap junction channels. The block of Cx40E9,13K I_j by 5 mM TPeA was reduced by approximately 50% relative to the model for wtCx40 (Fig. 2*D*). These data indicate that the E9 and E13 loci of Cx40 also affect TPeA permeation, but that some portion of the ion permeation pathway is also partially retained.

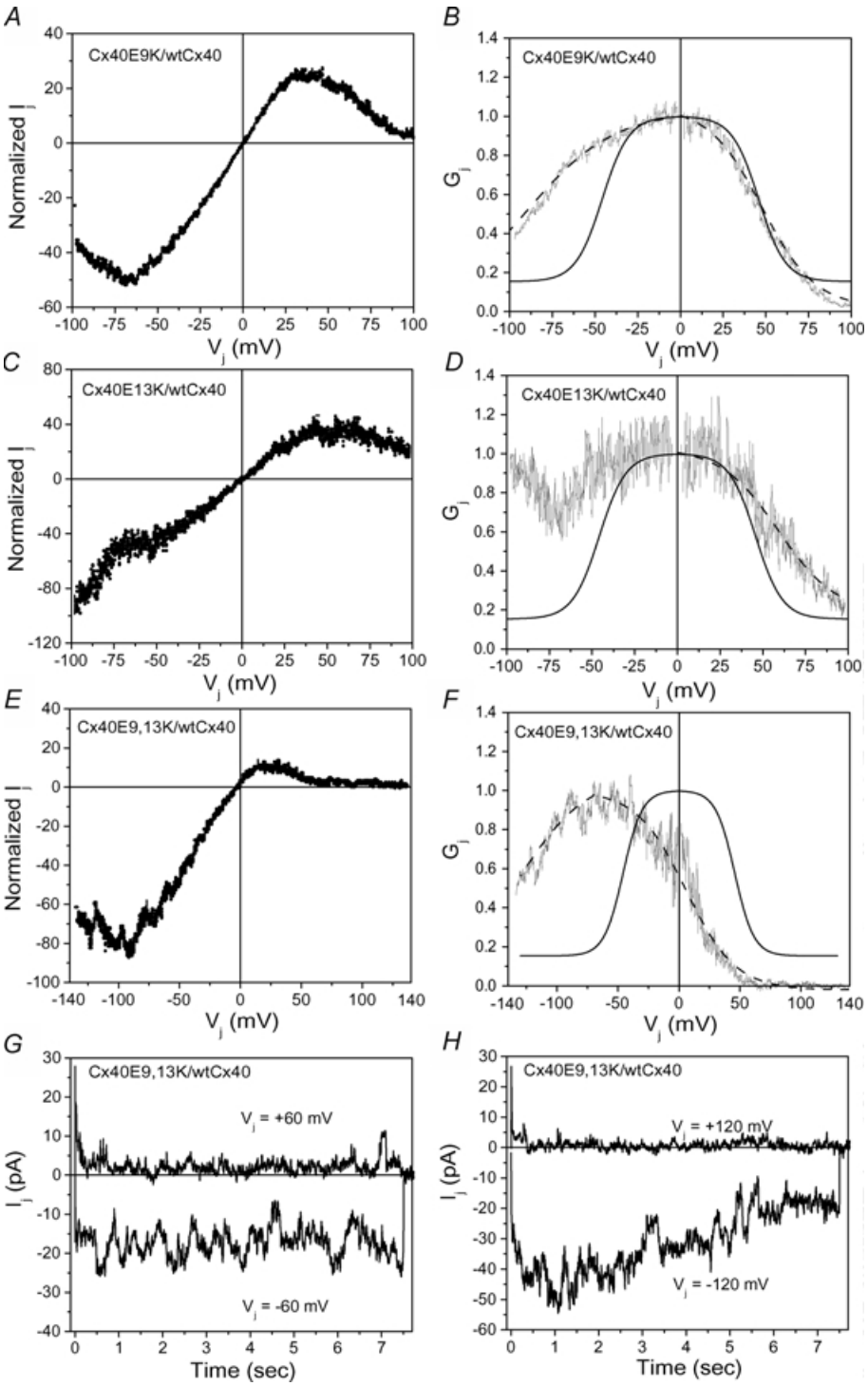

Figure 4. Heterotypic mutant Cx40/Cx40 I_j–V_j and G_j–V_j relationships
The steady-state I_j–V_j (*A*) and G_j–V_j (*B*) curves for the heterotypic Cx40E9K/wtCx40 gap junctions rectifies towards negative potentials. V_j is defined relative to the wtCx40 cell. The heterotypic Cx40E13K/wtCx40 gap junctions also rectifies towards negative potentials (*C*) with reduced V_j gating parameters (*D*). I_j–V_j (*E*) and G_j–V_j (*F*) relationships for Cx40E9,13K/wtCx40 heterotypic cell pairs demonstrating the rectifying behaviour of this gap junction without spermine. The values for the calculated Boltzmann curves for wtCx40 (continuous line) and the heterotypic Cx40E9K/wtCx40, Cx40E13K/wtCx40, Cx40E9,13K/wtCx40 (dashed lines) gap junctions are listed in Table 4. The heterotypic Cx40E9,13K/wtCx40 gap junctions closed with rapid decay kinetics at positive V_j values (+60 and +120 mV, *G* and *H*). At the corresponding negative V_j values, I_j was essentially ohmic (–60 mV) or exhibited biphasic gating properties (–120 mV) with slower kinetics and similar initial and steady-state values.

Table 2. Boltzmann equation values for the heterotypic Cx40 G_j–V_j curves

	Cx40E9K/wtCx40		Cx40E13K/wtCx40		Cx40E9,13K/wtCx40	
Parameter	$+V_j$	$-V_j$	$+V_j$	$-V_j$	$+V_j$	$-V_j$
G_{max}	1.0[a]	1.0[a]	NA	1.0[a]	1.0[a]	1.0[a]
$V_{½}$ (mV)	-90.0 ± 1.6	$+47.7 \pm 0.2$	NA	$+59.2 \pm 0.8$	-127.3 ± 5.0	$+5.8 \pm 0.3$
z	-1.18 ± 0.02	1.94 ± 0.02	NA	1.79 ± 0.07	-1.15 ± 0.06	1.24 ± 0.01
G_{min}	-0.07 ± 0.04	0.02 ± 0.01	NA	0.18 ± 0.02	0.11 ± 0.11	-0.02 ± 0.002

[a] G_{max} was fixed to a value of 1.0 since all junctional conductance measurements were normalized to the maximum g_j for each experiment. NA, not applicable; accurate Boltzmann fit could not be obtained for the data. Values are means ± S.E.M.

Homotypic mutant Cx40 gap junction V_j gating properties

To individually assess the effect of the E-to-K mutations of residues 9 and 13 on the V_j-dependent gating properties of Cx40 gap junctions, the steady-state V_j-dependent junctional conductance (g_j) curves of homotypic wtCx40, Cx40E9K, Cx40E13K, and Cx40E9,13K, were determined by varying V_j between + and –140 mV in 1 mV, 200 ms increments (Fig. 3*A*–*D*). The Cx40E13K mutation nearly abolished all V_j gating inherent to wtCx40 whereas the Cx40E9K and Cx40E9,13K homotypic gap junctions exhibited a typical Boltzmann distribution for the normalized steady-state junctional conductance–voltage (G_j–V_j) curves (Fig. 3, Table 1). The half-inactivation voltage ($V_{½}$) was larger in Cx40E9K than in Cx40E9,13K double point mutant gap junctions. The decrease in the $V_{½}$ is indicative of a relative reduction in the open probability for the Cx40E9,13K gap junctions, despite the additional loss of equivalent gating charges (z) evident in the Boltzmann distributions for these two mutant connexin gap junctions. The homotypic Cx40E9K gap junctions also exhibited the complete loss of any residual V_j-insensitive G_j (G_{min}). These data suggest that both the E9 and E13 loci contribute to the V_j gating properties of Cx40.

Heterotypic mutant/wild-type Cx40 gap junction V_j gating properties

Due to the inherent bilateral symmetry of all homotypic gap junctions, it becomes necessary to produce heterotypic gap junctions to assess the relative differences in the V_j gating properties of two related connexins. For this purpose, all three mutant Cx40 proteins were expressed in heterotypic combination with wtCx40 (Fig. 4). The steady-state junctional current–voltage (I_j–V_j) relationships for the Cx40E9K/wtCx40, Cx40E13K/wtCx40, and Cx40E9,13K/wtCx40 gap junctions all exhibit some degree of rectification, resulting in less current flow when V_j is positive in the wtCx40 cell. The corresponding G_j–V_j curves illustrate the asymmetry and the complex gating behaviour of these heterotypic gap junctions relative to homotypic wtCx40. In the Cx40E9K/wtCx40 and Cx40E9,13K/wtCx40 heterotypic cases, there was an increased $V_{½}$ and a reduced gating charge valence (z) evident at negative V_j values. The Cx40E13K/wtCx40 heterotypic gap junction could not be fitted with a single Boltzmann curve owing to the biphasic G_j curve observed at negative V_j values (Fig. 4*D*). The heterotypic single point E9K and E13K Cx40 mutants resulted in a 50% reduction in slope with little or no increase in the $V_{½}$ relative to wtCx40 at positive V_j values where the normal Cx40 V_j gating is expected to occur (Table 2). When both E-to-K point mutations were incorporated into the heterotypic Cx40 gap junction, the $V_{½}$ was reduced to near zero with a further reduction in the apparent valence to approximately one equivalent charge (Fig. 4*F*). G_j was also observed to reduce to zero at positive V_j in the heterotypic Cx40E9K/wtCx40 and Cx40E9,13K/wtCx40 gap junctions, consistent with the zero G_{min} properties of the Cx40E9K mutation. The reduced slope and increased $V_{½}$ at negative V_j and the low $V_{½}$ at positive V_j combine to produce a strongly rectifying Cx40E9,13K/wtCx40 gap junction reminiscent of the inwardly rectifying Kir2.1 potassium channel known to be blocked by spermine (Ficker *et al.* 1994; Lopatin *et al.* 1994). Hence, these results indicate that the E9K and E13K point mutations on the NT domain of Cx40 operate in concert to determine the V_j gating properties of Cx40.

Further support for the altered V_j gating properties of the Cx40E9,13K protein is evidenced by the macroscopic I_j recordings at reversed polarities in this heterotypic gap junction. At voltages near the G_{max}, i.e. –60 mV, very little gating is evident whereas the junction rapidly closes to near zero at the exact opposite V_j of +60 mV (Fig. 4*G*). At larger negative potentials, more complex gating behaviours were observed. It was regularly observed that I_j initially achieved similar values at both polarities of $V_j \geq \pm 100$ mV, only to close completely within

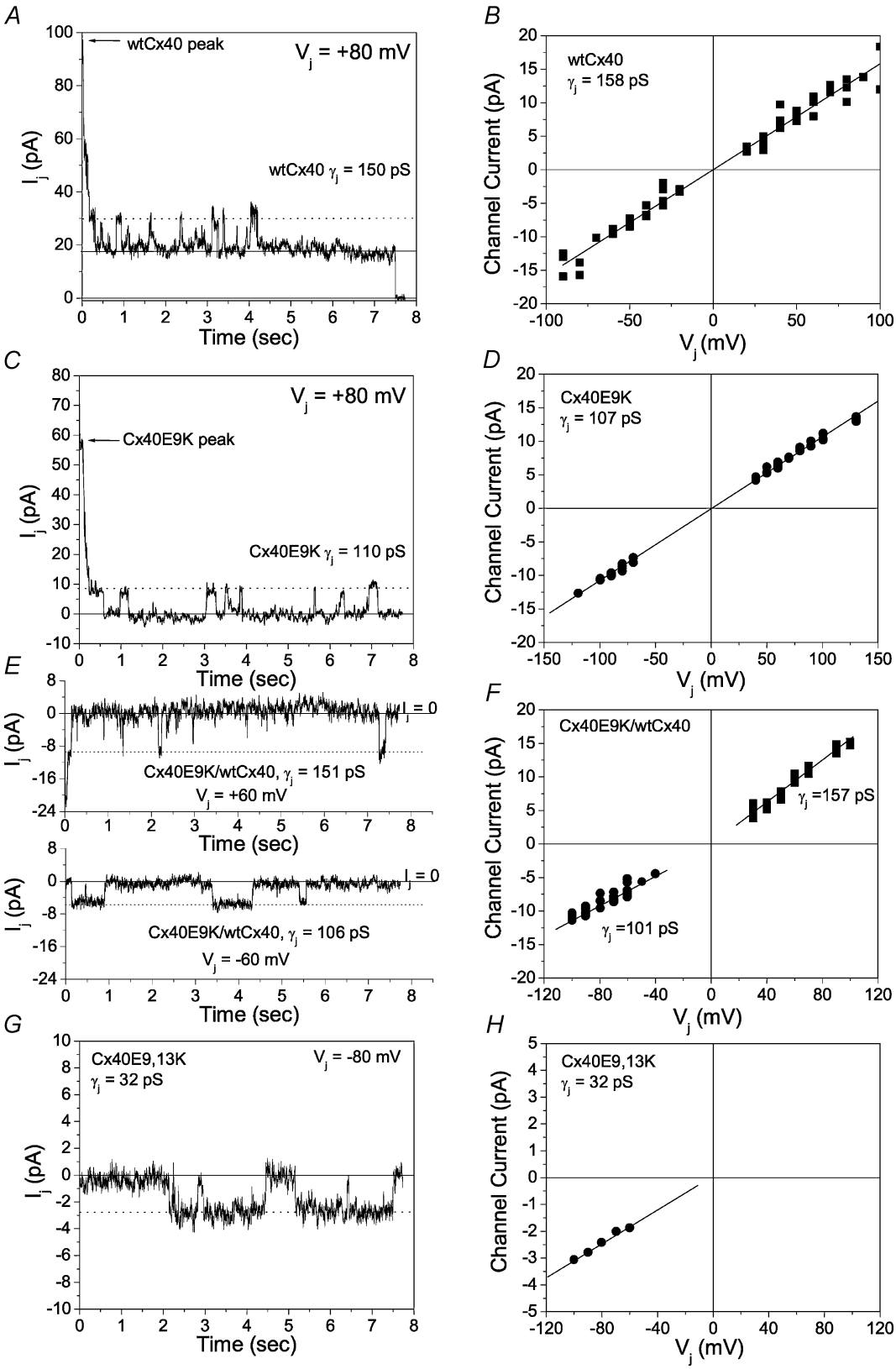

milliseconds at positive V_j (Fig. 4*H*). At the same large negative V_j values, I_j increased slowly and then decreased slightly to less than instantaneous values. These data indicate that closure of the V_j gate, rather than open channel current rectification, is the predominant mechanism for the current rectification at positive V_j values.

Conductance properties of mutant NT Cx40 single channels

It is of interest to know if the functional alterations in spermine blockade and V_j gating of Cx40 gap junctions associated with these acidic-to-basic charge substitutions at positions 9 and 13 have any effect on their single channel conductances. Figure 5*A* illustrates the typical response of a Cx40 gap junction to a V_j pulse of +80 mV, a rapid reduction in I_j to minimum steady-state values. Superimposed on this steady-state I_j baseline are discrete current fluctuations of about 12 pA in amplitude that correspond to a unitary conductance (γ_j) of 150 pS. The difference in the peak current amplitudes of the all points histogram from this and other V_j pulses were taken as the mean single channel current (I_j) values for the wtCx40 gap junction channel. The composite I_j–V_j relationship for the wtCx40 gap junction channel from three such experiments had a slope conductance of 157.9 ± 3.3 pS, consistent with earlier findings (Musa *et al.* 2001; Musa & Veenstra, 2003).

When the same procedure was applied to the homotypic Cx40E9K gap junction, channel currents of 8.8 pA were observed at +80 mV V_j (Fig. 5*C*). The Cx40E9K gap junction channel I_j–V_j relationship had a slope conductance of 107.1 ± 0.8 pS, a 32% reduction in γ_j relative to wtCx40 (Fig. 5*D*). The heterotypic combination of these two connexin channels revealed a modest rectification of the channel I_j–V_j relationship that distinctly correlated with the two γ_j values of the homotypic Cx40E9K and wtCx40 gap junction channels (Fig. 5*E* and *F*). This heterotypic gap junction acquired the channel conductance properties of the wtCx40 channel at positive V_j and of the Cx40E9K channel at negative V_j values. Single channel current fluctuations in homotypic Cx40E13K or heterotypic Cx40E9,13K/wtCx40 gap junctions were not resolved due to the lack of V_j gating and the reduced amplitude of the observed current fluctuations. However, unitary current fluctuations were observed on one occasion in a homotypic Cx40E9,13K cell pair (Fig. 5*G* and *H*). At a V_j of –80 mV, the current amplitude was less than 3 pA in this example. The slope conductance was 31.6 ± 1.9 pS, a mere 20% of the wtCx40 γ_j.

The low g_j recordings shown in Fig. 6 exemplify the channel conductance and gating properties of the mutant and wt Cx40 channels. The homotypic wtCx40 and Cx40E9K gap junctions exhibit obvious gating behaviour with increasing V_j characterized by large quantal current fluctuations associated with the closure of multiple channels (Fig. 6*A* and *B*). By comparison, quantal current fluctuations were not readily resolved in the lower noise recordings from similar low g_j Cx40E13K and Cx40E9,13K gap junctions (Fig. 6*C* and *D*). Again, inclusion of the E9K point mutation restores V_j gating properties to the mutant Cx40E13K gap junction (Fig. 6*D*), confirming previous observations about the V_j gating properties of these three homotypic mutant Cx40 gap junctions.

Effects of connexin43 K-to-E mutations

The effects of the K-to-E mutations of residues 9 and 13 on the V_j-dependent gating properties of Cx43,

Figure 5. I_j–V_j relationships for wt and mutant Cx40 gap junction channels
A, channel activity during a +80 mV, 7.5 s V_j pulse in a homotypic wtCx40 cell pair. Unitary current events corresponding to a 150 pS conductance channel (dashed line) were observed after I_j declined to a non-zero baseline (continuous line). *B*, unitary current amplitudes from 3 experiments on homotypic wtCx40 gap junctions. All amplitudes were determined from all points histograms from each V_j pulse. The average slope conductance was 158 pS. *C*, an example of I_j currents recorded during a +80 mV V_j pulse applied to a homotypic Cx40E9K cell pair. Note the occurrence of the 110 pS channel activity (dashed line) from a zero junctional current baseline (continuous line). *D*, the I_j–V_j relationship for this homotypic Cx40E9K channel with a slope conductance of 107.1 ± 0.8 pS. *E*, unitary channel activity observed in heterotypic Cx40E9K/wtCx40 cell pairs when pulsing the Cx40E9K cell (upper panel) or the wt Cx40 cell (lower panel) to –60 mV relative to the other cell in a heterotypic Cx40E9K/wtCx40 cell pair. $V_j = V_1 - V_2$ as always. The current amplitudes correspond to the wtCx40 channel at positive V_j and to the Cx40E9K channel at negative V_j values. *F*, the I_j–V_j relationship for this heterotypic Cx40E9K/wtCx40 gap junction channel with respective slope conductances of 101 pS and 157 pS at $-V_j$ and $+V_j$ values. *G*, an example of the channel activity observed from a homotypic Cx40E9,13K gap junction. Unitary events of 2.6 pA in amplitude (dashed line) were observed during the –80 mV V_j pulse. *H*, the slope conductance of the I_j–V_j from this experiment was 32 pS, approximately 20% of the wtCx40 channel conductance and one-third the γ_j of the Cx40E9K channel.

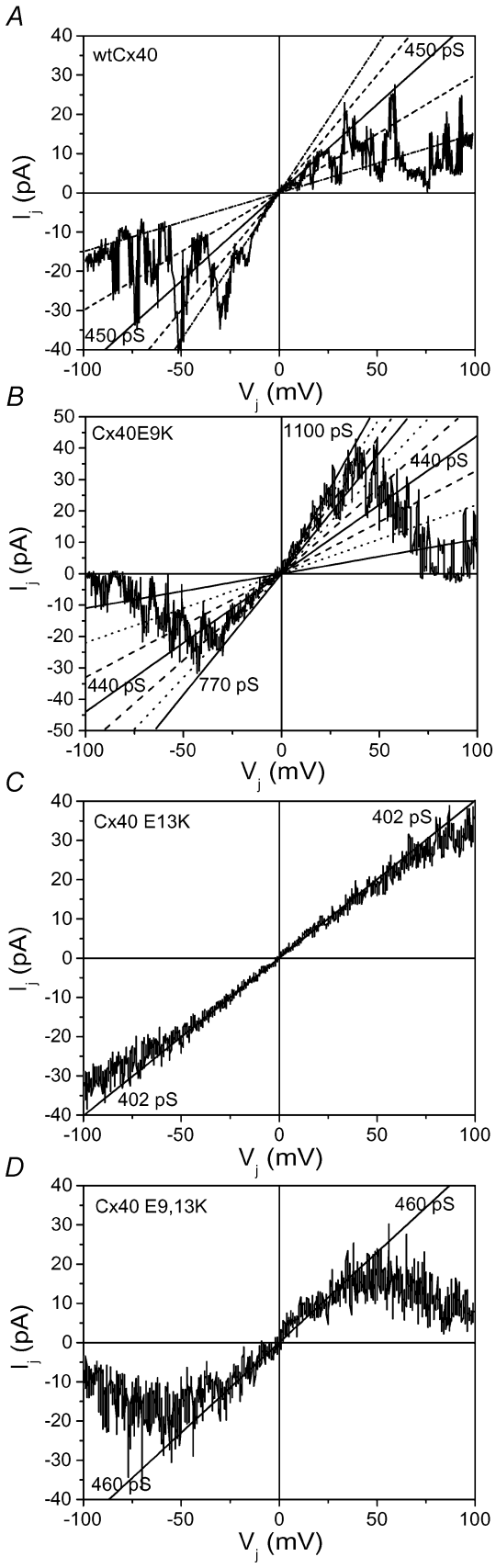

wtCx43, Cx43K9E, and Cx43K9,13E gap junctions were also determined. The Cx43K9E mutation only moderately reduced the equivalent gating charge of this homotypic gap junction relative to wtCx43 (Fig. 7, Table 3). In contrast to Cx40, the K9E mutation in Cx43 produced a dramatic increase in the G_{min} to more than double the wtCx43 value. Albeit the opposite effect to that observed at this exact locus in Cx40, the data again indicate a role for the NT domain in the formation of the G_{min} state. We were not able to obtain similar data with the Cx43K13E mutation since its expression levels were too high to permit reliable quantitative assessment of the V_j gating properties of this homotypic mutant gap junction (see Table 4). The V_j gating properties of Cx43 were apparently restored by the inclusion of the K13E substitution into the Cx43K9E mutant protein as indicated by the return to essentially wtCx43 V_j gating parameters. The reciprocal double point Cx43K9,13E mutant gap junctions remained insensitive to block by 2 mM spermine (data not shown).

In contrast to the heterotypic mutant Cx40/wtCx40 gap junctions, the combination of the Cx43K9E and Cx43K9,13E mutations with wtCx43 produced less dramatic alterations to the heterotypic I_j–V_j curves (Fig. 8*A* and *C*). V_j gating was evident at both V_j polarities in the heterotypic Cx43K9E/wtCx43 gap junction with a +30 mV shift in the apparent $V_{½}$ at positive V_j and a slope reduction of 50% at negative V_j (Fig. 8*A* and *B*, Tables 3 and 5). The G_{max} was also reduced by 50% at positive V_j and peaked near +70 mV. The G_{min} of 0.26 was only half of the apparent G_{max} at positive V_j values, consistent with the gating characteristics of the homotypic Cx43K9E gap junction. These changes were accompanied by a modest increase in the net gating charge valence of +0.6 relative to the homotypic Cx43K9E gap junctions. Conversely, the slope of the G_j–V_j curve at negative polarity was diminished relative

Figure 6. Continuous I_j–V_j curves depicting wt and mutant Cx40 channel behaviour
A, low g_j recording obtained during a 200 mV, 200 ms mV^{-1} V_j ramp in a homotypic wtCx40 cell pair. The gating activity of at least five 150 pS channels are evident (continuous line = 450 pS slope conductance, dashed lines ± 150 pS, dotted–dashed lines ± 300 pS from continuous line). *B*, a similar example from a homotypic Cx40E9K cell pair demonstrating the closure of more than 10 110 pS channels evident in this recording. *C*, conversely, no V_j gating is evident in a low g_j Cx40E13K cell pair. The current noise is of obviously lower amplitude than the wtCx40 or Cx40E9K recordings, making resolution of unitary channel fluctuations impossible. *D*, the Cx40E9,13K mutant gap junction retains the low amplitude noise fluctuations of the Cx40E13K mutation but some V_j gating is restored, consistent with the function of the Cx40E9K mutation.

to wtCx43, but with no apparent change in the $V_{½}$. As with the homotypic Cx43K13E gap junctions, the heterotypic Cx43K13E/wtCx43 expressed at too high a level to accurately determine the V_j gating properties of this gap junction (see Table 4).

Relative to the Cx43K9E/wtCx43 heterotypic combination, incorporation of the second point mutation into Cx43K9E significantly altered the gating behaviour of the Cx43K9,13E/wtCx43 heterotypic gap junctions. The G_{max} now occurred near –60 mV and exhibited a 50% increase in the slope with again no change in the $V_{½}$ of the G_j–V_j curve at negative V_j (Fig. 8*D*, Table 5). The heterotypic double mutant/wild-type Cx43 gap junction conducted more current than the Cx43K9E/wtCx43 counterpart when V_j exceeded +70 mV, apparently due to the diminution of V_j gating at large positive potentials and a higher relative G_{max} at lower V_j values. This was opposite to the effect of the reciprocal double point mutations observed in the heterotypic Cx40 gap junctions.

The wtCx43 channel has a lower conductance of approximately 97 pS (Wang & Veenstra, 1997). The channel current recordings and composite I_j–V_j relationship from three Cx43 cell pairs yielded similar results: mean $\gamma_j = 92.2 \pm 2.7$ pS (data not shown). In contrast to the double point mutations in Cx40, the Cx43K9,13E double point mutant protein still formed a homotypic gap junction channel with no discernable change in γ_j: mean $\gamma_j = 101.1 \pm 1.3$ pS (data not shown).

Discussion

The principal purpose of this investigation was to examine the possible role that naturally occurring E or K residue substitutions found in Cx40 and Cx43 play in the previously identified differential sensitivity to spermine block of these two cardiovascular gap junctions (Musa & Veenstra, 2003). Specific glutamate and aspartate residues play key roles in the polyamine block of the inward rectifier K^+ (e.g. Kir2.1) and the rod cyclic nucleotide gated (CNG) cation channels (Ficker *et al.* 1994; Lopatin *et al.* 1994; Guo & Lu, 2000*a*). For this reason, we specifically targeted cytoplasmic acidic amino acid residues in Cx40 that were not present in Cx43. The glutamatic acid residues that occur naturally at positions 9 and 13 on the amino terminal domain of Cx40 are two such residues (Fig. 1). The E9 and E13 loci of Cx40 were mutated individually and dually to the K9 and K13 residues found in Cx43 and examined for block by the unilateral addition of 2 mM spermine to homotypic cell pairs. This concentration of spermine produced maximal block in wtCx40 gap junctions, but only nominal amounts of block in the Cx40E13K and Cx40E9,13K mutant Cx40 gap junctions (Fig. 2). There also appeared to be a lower amount of block in the Cx40E9K gap junctions, characterized by a reduced

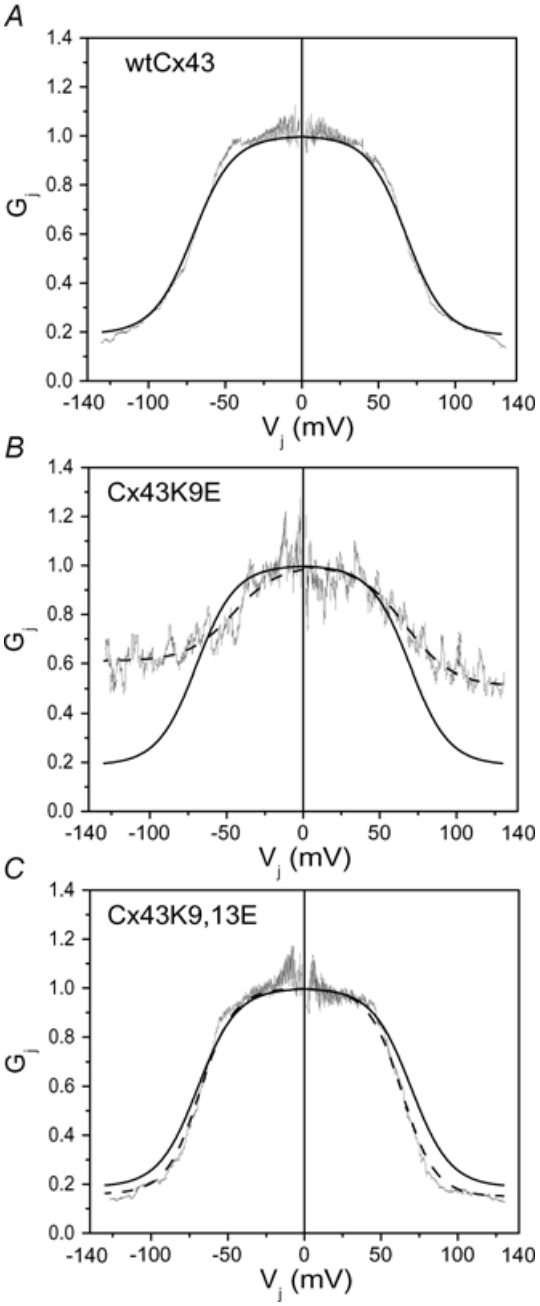

Figure 7. G_j–V_j curves for wt and mutant Cx43 gap junctions
A, the V_j gating behaviour of wtCx43 gap junctions (continuous line) is illustrated using the same V_j protocol as Cx40 (see Table 3 for details). *B*, the G_{min} was more than double in the mutant Cx43K9E gap junctions (dashed line) with little change in the $V_{½}$ or gating charge compared to wtCx43 (continuous line). *C*, G_j–V_j curves depicting the apparent similar V_j gating behaviour of the Cx43K9,13E mutant gap junctions (dashed line) relative to wtCx43 (continuous line).

Table 3. Boltzmann equation values for the Cx43 G_j–V_j curves

	wtCx43		Cx43K9E		Cx43K9,13E	
Parameter	$-V_j$	$+V_j$	$-V_j$	$+V_j$	$-V_j$	$+V_j$
G_{max}	1.0[a]	1.0[a]	1.0[a]	1.0[a]	1.0[a]	1.0[a]
$V_{½}$ (mV)	-69.6 ± 2.0	$+69.6 \pm 2.0$	-45.7 ± 0.5	$+66.8 \pm 1.5$	-68.1 ± 0.1	$+63.6 \pm 0.1$
z	-2.37 ± 0.07	2.37 ± 0.07	-2.05 ± 0.06	1.99 ± 0.08	-2.74 ± 0.02	2.75 ± 0.02
G_{min}	0.19 ± 0.004	0.19 ± 0.004	0.61 ± 0.002	0.51 ± 0.02	0.16 ± 0.002	0.15 ± 0.001

[a] G_{max} was fixed to a value of 1.0 since all junctional conductance measurements were normalized to the maximum g_j for each experiment. Values are means ± S.E.M.

spermine association at low voltages compared to wtCx40 gap junctions. There was no effective spermine block present at concentrations below 0.5 mM or below 20 mV V_j with the Cx40E9K channel, making the 'equivalent electrical distance' calculations as previously determined for the wtCx40 gap junction impossible (Musa & Veenstra, 2003). We conclude that both E9 and E13 contribute to the block of Cx40 I_j by 2 mM spermine, with E13 being required for this inhibitory activity.

Despite the virtual elimination of spermine block by the E9K and E9,13K mutations in Cx40, approximately 50% of the block by 5 mM TPeA remained with this mutation (Fig. 2*D*, Musa *et al.* 2001). TPeA block was postulated to occur by steric hindrance, i.e. the approximate pore and ionic diameters are effectively equivalent at a narrow internal restriction site. Both TPeA and spermine inhibit Cx40 I_j by reducing channel open probability to near zero with little or no effect on the main state conductance of the single channel conductance. This type of block resembles altered channel gating more than 'flickery' permeation block and is associated with prolonged association times with the channel, consistent with bimolecular binding. The polyamine block of the Kir2.1 channel also exhibits some degree of a 'gating' type of block atypical of the flickery 'open' channel block associated with truly impermeant ions (Lopatin *et al.* 1995; Lee *et al.* 1999; Guo & Lu, 2000*b*). The elimination of spermine block accompanied by the partial retention of TPeA block could be explained by reduced monovalent cation partitioning into the Cx40 pore with no change in the internal pore diameter. We have yet to perform the necessary ionic substitution experiments to estimate the relative cation/anion conductances and pore diameters of the mutant Cx40 and Cx43 channels (Veenstra, 1996; Beblo & Veenstra, 1997; Wang & Veenstra, 1997).

Interestingly, the E9K point mutation reduced the gating charge of Cx40 by ∼25% while the E13K effaced the typical Boltzmann distribution of the G_j–V_j curve (Fig. 3, Table 1). Each homologous Cx40 K-for-E or Cx43 E-for-K substitution results in a net valence change of ±2 per locus. Yet the homotypic E9K and E9,13K mutations in Cx40 reduced the apparent gating charge valence by only 1 and 2 equivalent charges, respectively. The homotypic E13K mutation effectively eliminated the V_j gating of Cx40 altogether, as it did to the blockade by spermine. The E9K mutation similarly produced only a 32% diminution of Cx40 γ_j but, when combined with the E9K mutation, it resulted in an 80% reduction in γ_j (Figs 5 and 6). The E13K mutation γ_j could not be assessed individually.

It is possible that the E13K substitution, which results in a neutral E12K13 locus instead of the rare occurrence of a highly acidic double glutamate locus at the midpoint of the connexin amino terminal domain sequences, is vital to the structural conformation of this putative pore-forming domain. The E9K locus, by virtue of its more internal location according to the domain-hinge-domain motif proposed by Purnick *et al.* (2000*a*), may produce a lesser effect since the presence or absence of the E12,13 locus closer to the cytoplasm plays a greater role in determining the partitioning of permeable cations into the mouth of the channel. For this to be true, the charge density must also be greater at the E12,13 site, suggesting that the pore diameters are not dramatically ($<\sqrt{2}$) different at these two sequential sites on the Cx40 NT domain. Whether these effects are the result of point charge reversal or disruption of secondary structure can be further assessed by conservative (D) or polar neutral (Q, N) amino acid substitutions at positions 9 and 13 of Cx40.

The present model for V_j-dependent gating assumes that there are two identical gates in series but with the opposite orientation on each side of a homotypic gap junction channel (Harris *et al.* 1981; Verselis *et al.* 1994). The 'voltage sensor' for the 'fast' V_j-dependent gating was localized within the NT domain of the connexins. This voltage-sensing domain was postulated to reside within the V_j field owing to a highly conserved glycine hinge at position 12 originally identified in Cx26 (Purnick *et al.* 2000*a*). Recent evidence has indicated that only one V_j gate needs to close to occlude the pore (Oh *et al.* 2000). Furthermore, charged amino acid substitutions up to

Table 4. Average junctional conductances per experimental group

Exp. group	Mean g_j (nS)	± S.D.	N	Figure no.
Cx40 +2 mM spermine	4.38	±2.37	3	2*A–C*
Cx40E9K +2 mM spermine	5.03	±4.44	3	2*B*
Cx40E13K +2 mM spermine	3.72	±2.59	3	2*B*
Cx40E9,13K +2 mM spermine	2.26	±0.82	3	2*C*
Cx40E9,13K +5 mM TPeA	2.59	±2.62	3	2*D*
Cx40	1.29	±1.04	3	3*A*
Cx40E9K	2.48	±1.82	3	3*B*
Cx40E13K	2.15	±1.35	4	3*C*
Cx40E9,13K	1.83	±0.27	3	3*D*
Cx43	1.33	±0.83	3	7*A*
Cx43K9E	1.37	±0.83	4	7*B*
Cx43K13E	31.4	±12.3	14	—
Cx43K9,13E	2.90	±1.45	3	7*C*
Cx40E9K/wtCx40	2.17	±1.94	3	4*A* and *B*
Cx40E13K/wtCx40	0.50	±0.35	3	4*C* and *D*
Cx40E9,13K/wtCx40	1.45	±1.65	4	4*E* and *F*
Cx43K9E/wtCx43	2.16	±1.09	3	8*A* and *B*
Cx43K13E/wtCx43	17.3	±3.3	3	—
Cx43K9,13E/wtCx43	3.98	±1.51	2	8*C* and *D*

Table 5. Boltzmann equation values for the heterotypic Cx43 G_j–V_j curves

	Cx43K9E/wtCx43		Cx43K9,13E/wtCx43	
Parameter	$-V_j$	$+V_j$	$-V_j$	$+V_j$
G_{max}	1.0[a]	0.58 ± 0.002	1.0[a]	NA
$V_{½}$ (mV)	−67.8 ± 0.2	+87.6 ± 0.2	−69.3 ± 0.1	NA
z	−1.16 ± 0.007	2.66 ± 0.06	−3.65 ± 0.03	NA
G_{min}	0.12 ± 0.002	0.26 ± 0.002	0.16 ± 0.001	NA

[a] G_{max} was fixed to a value of 1.0 since all junctional conductance measurements were normalized to the maximum g_j for each experiment. Values are means ± S.E.M. NA, not applicable; accurate Boltzmann fit could not be obtained for the data.

position 10 of the NT domain of Cx26 can alter the voltage gating polarity and sensitivity of this connexin (Purnick *et al.* 2000*b*). Pairing two connexins with opposite voltage polarities for V_j-dependent inactivation in a heterotypic configuration (each half of the gap junction being composed of a different connexin) results in a rectifying G_j–V_j curve due to the asymmetric gating and channel conductance properties (Verselis *et al.* 1994; Bukauskas *et al.* 1995). Cx40 and Cx43 are similarly proposed to close with positive and negative V_j polarities, respectively, which are also of opposite sign to the charged amino acid residues on the NT domain (Valiunas *et al.* 2000).

Our data from the homotypic and heterotypic pairings of the Cx40E9 (and/or)13K mutants with themselves or wild-type Cx40 confirm that there are alterations in the V_j gating properties of these gap junctions (Figs 3 and 4, Tables 1 and 2). The heterotypic combinations of the Cx40 E9K and E13K mutations with wtCx40 produced asymmetric G_j–V_j curves with reduced slopes at both polarities and shifted $V_{½}$ values. The rectifying I_j–V_j curve of the heterotypic wtCx40/Cx40E9,13K gap junction, obtained in the absence of spermine, strongly resembled the *I–V* curve for wtCx40, obtained in the presence of 2 mM unilateral spermine, and the inward rectifier Kir2.1 channel in the presence of 10–100 μM intracellular spermine (Ficker *et al.* 1994; Lopatin *et al.* 1994), further supporting the hypothesis that these E9,13 loci are critical to the polyamine block of the wtCx40 gap junction channel (Fig. 4*E*). All of the heterotypic results were reported with V_j relative to the wtCx40 cell. If it is assumed that the positive V_j gating parameters reflect the V_j gating properties of the wtCx40 hemichannel relative to the mutant hemichannel, then both the E9K and E13K substitutions reduce the valence by 1 while only the E13K mutation affects the open–closed probability equilibrium at positive V_j values. Combining both mutations in Cx40 shifts the $V_{½}$ by negative 40 mV with only a slight additional reduction (0.5) in valence.

One hypothesis that could account for the differential functional effects of these two charge reversal mutations is that the combination of both point mutations reverses the V_j gating polarity of Cx40 from positive to negative. Each individual mutation reduces the positive gating relative to wtCx40 and the Cx40E9,13K double mutation effectively reverses it. One cannot definitively distinguish between a simple electrostatic voltage shift towards more negative V_j values and reversal of the V_j gating polarity in the Cx40E9,13K mutant gap junctions, but the lack of any shift in the G_{max} in the heterotypic steady-state G_j–V_j curves by both single point mutations does not favour an electrostatic mechanism. The proposed positive V_j gating polarity of wtCx40 hemichannels is further supported by the observation of the wtCx40 γ_j at positive V_j values (Fig. 5; Valiunas *et al.* 2000). The observation of the mutant Cx40E9K γ_j at negative V_j values (relative to wtCx40) is indicative of an operative positive V_j gate in the mutant Cx40E9K hemichannel. At all positive V_j values, the ohmic instantaneous I_j decayed essentially to zero within 1 s (Fig. 4*G* and *H*). The brief appearance of a subconductance state in these records is consistent with the gating of the wtCx40 channels at positive V_j while the complete closure of the Cx40E9,13K/wtCx40 gap junction is consistent with the zero G_{min} state attributed to the Cx40E9K mutation. The zero G_{min} state was also accomplished by the complete closure of several

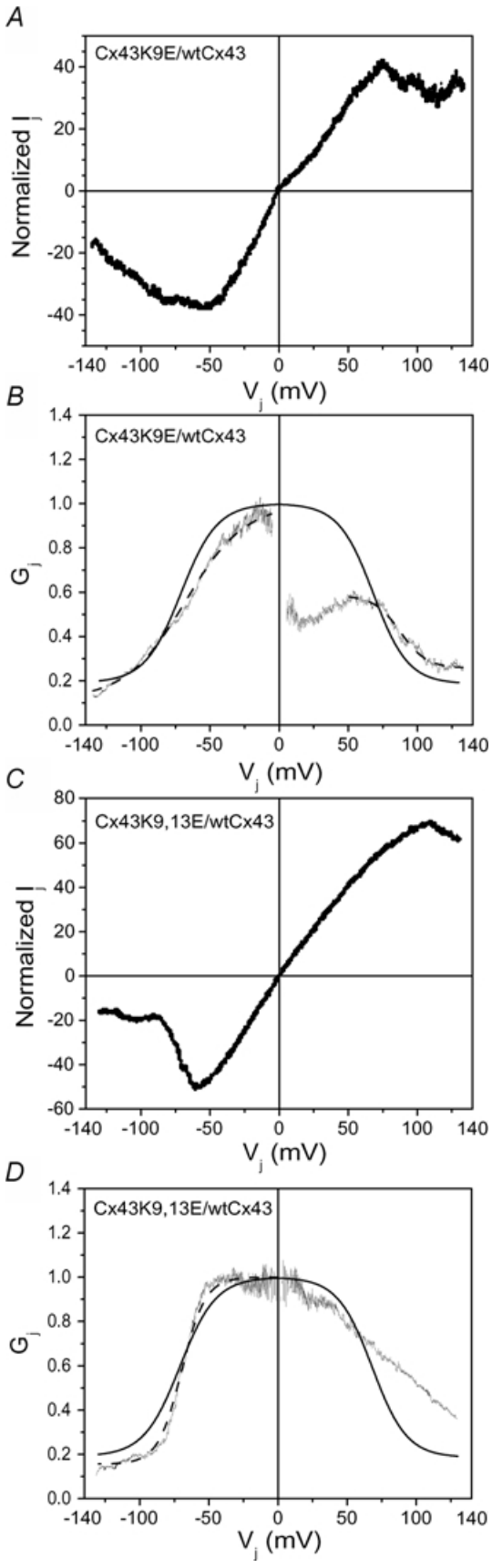

homotypic Cx40E9K gap junction channels (Fig. 5*C* and *E*) without the occurrence of a subconductance state as observed in the presence of wtCx40 in the heterotypic gap junctions (Fig. 4*G* and *H*).

The complex biphasic gating behaviour observed at −120 mV in the Cx40E9,13K/wtCx40 gap junctions suggests that the mutant Cx40E9,13K hemichannel possess bipolar V_j gating properties since characteristics of the mutant Cx40 hemichannel are observed at both negative and positive V_j values. The sequence of positive and negative amino acids in the Cx40E9,13K mutant protein is DKEK, similar to the DKDK sequence found in wtCx43 at positions 3, 9, 12, and 13. These results suggest that all of the point charges do not contribute equally to the gating charge valence of Cx40. Since all of the Boltzmann distribution measurements were obtained relative to the homologous mutant Cx40 or wtCx40 protein, they reflect relative differences in the transjunctional voltage distribution across a symmetric or asymmetric Cx40 gap junction. Hence, each charge reversal mutation in Cx40 may account for an apparent unitary reduction in gating charge valence, but the double E-to-K mutation may at least partially reverse the gating polarity of Cx40. V_j polarity reversal would be expected to increase the cooperativity of channel closure at positive V_j in a contingent gating scheme as originally proposed by Harris *et al.* (1981).

We postulate that the V_j gradient can drop entirely across the E9,13K loci of Cx40 as indicated by the complete inhibition of g_j by spermine, which certainly interacts with these sites, and the zero G_{min} observed with the inclusive Cx40E9K homotypic and heterotypic gap junctions. These alterations in V_j gating occur despite the conservation of an aspartate residue at position 3 (D3) in Cx40 and Cx43 that is analogous to the D or N substitutions found at position 2 owing to the addition of a glycine at position 2 in both Cx40 and Cx43. Furthermore, the glycine hinge at position 12 in Cx26 and Cx32 is absent in Cx40 and Cx43 where the analogous position 13 is occupied by the respective E or K residue (Verselis *et al.* 1994; Purnick *et al.* 2000*a*; Harris, 2002). This possible interpretation

Figure 8. Heterotypic mutant Cx43/Cx43 I_j–V_j and G_j–V_j relationships
The steady-state I_j–V_j (*A*) and G_j–V_j (*B*) relationships for the heterotypic Cx43K9E/wtCx43 gap junctions depicting rectification favouring negative V_j values. The steady-state G_j–V_j relationship illustrates the positive shift in the $V_{1/2}$ and the reduced slope for the negative V_j gating observed in this heterotypic gap junction (dashed line, see Table 5) relative to wtCx43 (continuous line). Inclusion of the second point mutation to form the heterotypic Cx43K9,13E/wtCx43 gap junction (*C* and *D*) increased the slope of V_j gating at negative V_j values (dashed line, see Table 5).

is called to question by the observations in Cx43 where the reciprocal K9,13E double point mutation did not confer spermine block to the Cx43 gap junction. The results were also not as obvious in regard to the homotypic and heterotypic V_j gating properties of the Cx43 mutants (Figs 7 and 8, Tables 3 and 5). The $V_{½}$ was negligibly altered while the valence was, respectively, decreased or increased by approximately 0.5 or 1.0 in the homotypic or heterotypic Cx43K9E and Cx43K9,13E combinations with wtCx43. This is in contrast to the sublinear additive decreases in valence observed with the reciprocal Cx40 mutations. Similarly, significant changes in Cx43 γ_j were not observed with the K9,13E mutations. If there was any effect at all, the Cx43K9,13E mutation resulted in at most a 10% increase in Cx43 γ_j. However, as the sequence information in Fig. 1 indicates, there are other amino acid differences, albeit not involving precise reciprocal charge substitutions, between the amino terminal domains of Cx40 and Cx43 that may also contribute to the overall structure of the putative 'polyamine receptor' of Cx40. It is also possible that interdomain interactions that have yet to be defined are important in this inhibitory bimolecular interaction.

It was proposed, at least for Cx43, that the fast V_j gate operates by a ball-and-chain mechanism where the CT domain forms the subcondutance state by interacting with a receptor associated with the channel pore (Moreno *et al.* 2002). The Cx40E9K gap junction channel closed completely with rapid kinetics and with both fast (< 10 ms) and slow (> 10 ms) transition times whereas the Cx43K9E gap junction had an increased G_{min}. These data suggest that the position 9 locus is somehow integrally involved in determining the channel's ability to close. The ability of spermine to completely inhibit Cx40 g_j is consistent with the hypothesis that spermine occludes the Cx40 pore by serving as an exogenous inactivation particle in its interactions with the NT domain of Cx40. The CT domain of Cx43, however, does not bind to the NT domain of Cx43. Instead it interacts with the second half of the cytoplasmic loop domain of Cx43 nearest to the third transmembrane domain and is involved in the pH gating of this gap junction (Duffy *et al.* 2002). We have alternatively proposed that the actions of the CT domain on fast V_j gating occur through intermediate interactions and that some other portion of the connexin molecule serves as the endogenous inactivation particle (Veenstra, 2003). The structure and function of the NT domains of Cx40 and Cx43 should continue to be investigated using both site-directed mutagenic and chimeric domain-swapping approaches. It is not clear how each locus of point charge contributes to the total gating charge of Cx40 and Cx43 except that the results are obviously not linear. The conserved D3 and D/E12 point charges on the NT domains of Cx40 and Cx43 should also be examined in this context to determine what role they play in the V_j-dependent closure and how pore occlusion is accomplished in these gap junctions.

References

Abrams CJ, Davies NW, Shelton PA & Stanfield PR (1996). The role of a single aspartate residue in ionic selectivity and block of a murine inward rectifier K^+ channel Kir2.1. *J Physiol* **493**, 643–649.

Beblo DA & Veenstra RD (1997). Monovalent cation permeation through the connexin40 gap junction channel: Cs, Rb, K, Na, Li, TEA, TMA, TBA and effects of anions Br, Cl, F, acetate, aspartate, glutamate, and NO3. *J General Physiol* **109**, 509–522.

Beblo DA, Wang H-Z, Beyer EC, Westphale EM & Veenstra RD (1995). Unique conductance, gating, and selective permeability properties of gap junction channels formed by connexin40. *Circ Res* **77**, 813–822.

Bowie D & Mayer ML (1995). Inward rectification of both AMPA and kainate subtype glutamate receptors generated by polyamine-mediated ion channel block. *Neuron* **15**, 453–462.

Bukauskas FF, Elfgang C, Willecke K & Weingart R (1995). Biophysical properties of gap junction channels formed by mouse connexin40 in induced pairs of transfected human HeLa cells. *Biophys J* **68**, 2289–2298.

Chao J, Seiler N, Renault J, Kashiwagi K, Masuko T, Igarashi K & Williams K (1997). N^1-dansyl-spermine and N^1-(n-octanesulfonyl)-spermine, novel glutamate receptor antagonists: block and permeation of N-methyl-D-aspartate receptors. *Mol Pharmacol* **51**, 861–871.

Duffy HS, Sorgen PL, Girvin ME, O'Donnell P, Coombs W, Taffet SM, Delmar M & Spray DC (2002). pH-dependent intramolecular binding and structure involving Cx43 cytoplasmic domain. *J Biol Chem* **277**, 36706–36714.

Ficker E, Taglialatela M, Wible BA, Henley CM & Brown AM (1994). Spermine and spermidine as gating molecules for inward rectifier K+ channels. *Science* **266**, 1068–1072.

Guo D & Lu Z (2000*a*). Mechanism of cGMP-gated channel block by intracellular polyamines. *J General Physiol* **115**, 783–797.

Guo D & Lu Z (2000*b*). Mechanism of IRK1 channel block by intracellular polyamines. *J General Physiol* **115**, 799–813.

Harris AL (2001). Emerging issues of connexin channels: Biophysics fills the gap. *Quart Rev Biophys* **34**, 325–472.

Harris AL (2002). Voltage-sensing and substate rectification: Moving parts of connexin channels. *J General Physiol* **119**, 165–169.

Harris AL, Spray DC & Bennett MVL (1981). Kinetic properties of a voltage-dependent junctional conductance. *J General Physiol* **77**, 95–117.

Hume RI, Dingeldine R & Heinemann SF (1991). Identification of a site in glutamate receptor subunits that controls calcium permeability. *Science* **253**, 1028–1031.

Hurst RS, Latorre R & Stefani E (1995). External barium block of *Shaker* potassium channels: evidence for two binding sites. *J General Physiol* **106**, 1069–1087.

Kashiwagi K, Fukuchi J, Chao J, Igarashi K & Williams K (1996). An aspartate residue in the extracellular loop of the N-methyl-D-aspartate receptor controls sensitivity to spermine and protons. *Mol Pharmacol* **49**, 1131–1141.

Kwong KF, Schuessler RB, Green KG, Laing JG, Beyer EC, Boineau JP & Saffitz JE (1998). Differential expression of gap junction proteins in the canine sinus node. *Circ Res* **82**, 604–612.

Laing JG & Beyer EC (1995). The gap junction protein connexin43 is degraded by the ubiquitin proteosome pathway. *J Biol Chem* **270**, 26399–26403.

Lampe PD & Lau AF (2000). Regulation of gap junctions by phosphorylation of connexins. *Arch Biochem Biophys* **384**, 205–215.

Lee J-K, John SA & Weiss JN (1999). Novel gating mechanism of polyamine block in the strong inward rectifier K channel Kir2.1. *J General Physiol* **113**, 555–563.

Lopatin AN, Makhina EN & Nichols CG (1994). Potassium channel block by cytoplasmic polyamines as the mechanism of intrinsic rectification. *Nature* **372**, 366–369.

Lopatin AN, Makhina EN & Nichols CG (1995). The mechanism of inward rectification of potassium channels: 'Long-pore plugging' by cytoplasmic polyamines. *J General Physiol* **106**, 923–955.

Lu Z & Ding L (1999). Blockade of a retinal cGMP-gated channel by polyamines. *J General Physiol* **113**, 35–43.

Moreno AP, Chanson M, Anumonwo J, Scerri I, Gu H, Taffet SM & Delmar M (2002). Role of the carboxyl terminal of connexin43 in transjunctional fast voltage gating. *Circ Res* **90**, 450–457.

Mori H, Masaki H, Yamakura T & Mishina M (1992). Identification by mutagenesis of a Mg^{2+}-block site of the NMDA receptor channel. *Nature* **358**, 673–675.

Musa H, Gough JD, Lees WJ & Veenstra RD (2001). Ionic blockade of the rat connexin40 gap junction channel by large tetraalkylammonium ions. *Biophys J* **81**, 3253–3274.

Musa H & Veenstra RD (2003). Voltage-dependent blockade of connexin40 gap junctions by spermine. *Biophys J* **84**, 205–219.

Oh S, Abrams CK, Verselis VK & Bargiello TA (2000). Stoichiometry of transjunctional voltage-gating polarity reversal by a negative charge substitution in the amino terminus of a connexin32 chimera. *J General Physiol* **116**, 13–31.

Purnick PEM, Benjamin DC, Verselis VK, Bargiello TA & Dowd TL (2000*a*). Structure of the amino terminus of a gap junction protein. *Arch Biochem Biophys* **381**, 181–190.

Purnick PE, Oh S, Abrams CK, Verselis VK & Bargiello TA (2000*b*). Reversal of the gating polarity of gap junctions by negative charge substitutions in the N-terminus of connexin32. *Biophys J* **79**, 2403–2415.

Root MJ & MacKinnon R (1993). Identification of an external divalent cation-binding site in the pore of a cGMP-activated channel. *Neuron* **11**, 459–466.

Tabor CW & Tabor H (1984). Polyamines. *Annu Rev Biochem* **53**, 749–790.

Uehara A, Fill M, Vélez P, Yasukochi M & Imanaga I (1996). Rectification of rabbit polyamine receptor current by endogenous polyamines. *Biophys J* **71**, 769–777.

Valiunas V, Weingart R & Brink PR (2000). Formation of heterotypic gap junction channels by connexins 40 and 43. *Circ Res* **86**, e42–e49.

Vallette F, Mege E, Reiss A & Adesnik M (1989). Construction of mutant and chimeric genes using the polymerase chain reaction. *Nucl Acids Res* **17**, 723–733.

Veenstra RD (1996). Size and selectivity of gap junction channels formed from different connexins. *J Bioenergetics Biomembranes* **28**, 327–337.

Veenstra RD (2000). Ion permeation through connexin gap junction channels: effects on conductance and selectivity. In *Gap Junctions. Molecular Basis of Cell Communication in Health and Disease. Current Topics in Membranes*, vol. 49, ed. Peracchia C, pp. 95–129. Academic Press, New York.

Veenstra RD (2001). Voltage clamp limitations of dual whole-cell gap junction current and voltage recordings. I. Conductance measurements. *Biophys J* **80**, 2231–2247.

Veenstra RD (2003). Towards gap junction channel structure. *Recent Res Devel Biophys* **2**, 65–94.

Verselis V, Ginter CS & Bargiello TA (1994). Opposite voltage gating polarities of two closely related connexins. *Nature* **368**, 348–351.

Wang HZ & Veenstra RD (1997). Monovalent ion selectivity sequences of the rat connexin43 gap junction channel. *J General Physiol* **109**, 491–507.

Wible BA, Taglialatela M, Ficker E & Brown AM (1994). Gating of inwardly rectifying K^+ channels localized to a single negatively charged residue. *Nature* **371**, 246–249.

Williams K (1997). Interactions of polyamines with ion channels. *Biochem J* **325**, 289–297.

Yang J, Jan YN & Jan LY (1995). Control of rectification and permeation by residues in two distinct domains in an inward rectifier K^+ channel. *Neuron* **14**, 1047–1054.

Acknowledgements

We thank Bogdan Goc for his technical assistance in preparing the mutant plasmids. We thank Dr Peter R. Brink, Department of Physiology and Biophysics, SUNY Stony Brook, NY for his helpful discussions. This work was supported by National Institutes of Health grants HL-42220 to R.D.V and HL-45466 to E.C.B and R.D.V.